Title:

MULTISCALE COMPUTATIONAL ANALYSIS OF THE BIOELECTRIC CONSEQUENCES OF MYOCARDIAL ISCHAEMIA AND INFARCTION

Authors:

Jose M. Ferrero[1], Beatriz Trenor[1], Lucia Romero[1]

Institution:

[1] I3BH, Universitat Politècnica de València

Address:

[1] Instituto I3BH, Universitat Politècnica de València, Camino de Vera s/n, 46022 Valencia, Spain

Corresponding author:

Jose M. Ferrero

Universitat Politècnica de València - Instituto I3BH

Camino de Vera s/n,

46022 Valencia, Spain.

Phone number: +34-96-3877007 (ext. 67037).

E-mail: cferrero@gbio.i3bh.es

Abstract

Ischaemic heart disease is considered as the single most frequent cause of death, provoking more than 7,000,000 deaths every year worldwide. A high percentage of patients experience sudden cardiac death, caused in most cases by tachyarrhythmic mechanisms associated to myocardial ischaemia and infarction. These diseases are difficult to study using solely experimental means due to their complex dynamics and unstable nature. In the past decades, integrative computational simulation techniques have become a powerful tool to complement experimental and clinical research when trying to elucidate the intimate mechanisms of ischaemic electrophysiological processes and to aid the clinician in the improvement and optimization of therapeutic procedures. The purpose of this paper is to briefly review some of the multiscale computational models of myocardial ischaemia and infarction developed in the past twenty years, ranging from the cellular level to whole-heart simulations.

Keywords

ischaemia; infarction; computer simulations; mathematical models; reentrant arrhythmias

INTRODUCTION

Ischaemia and infarction

Ischaemic heart disease is considered as the single most frequent cause of death, provoking more than 7,000,000 deaths every year worldwide.[1,2] A high percentage of patients suffering ischaemic heart disease experience sudden cardiac death,[3] with over to 450,000 cases being reported in the U.S. annually.[4] Almost 70% of them were probably caused by tachyarrhythmias associated to myocardial ischaemia.[4,5] It is therefore not surprising that an enormous body of research is being devoted to investigate the mechanisms underlying the relationship between myocardial ischaemia/infarction and arrhythmias.

Myocardial ischaemia usually results from the occlusion of a coronary artery, and can be defined as a condition in which the blood supply to heart cells is insufficient to meet their metabolic demands.[6] During the first 15 minutes after coronary artery occlusion ("phase 1A ischaemia"), the heart suffers profound metabolic and electrophysiological changes at different scales. At the subcellular level, electrolyte concentrations change, ATP and oxygen levels decline and pH decreases.[7] At the cellular level, ion channel activity changes, resting potential becomes less negative, action potential duration (APD) shortens, upstroke velocity decreases and cells loose excitability.[7] At the organ level, conduction velocity (CV) decreases and severe tachyarrhythmias may easily develop.[8,9] During the period that follows ("phase 1B ischaemia", 15-45 minutes post occlusion), cellular uncoupling develops,[10] ischaemic tissue becomes inexcitable and arrhythmias may re-appear after a safe period of several minutes.[11,12]

When the acute phase terminates, the infarcted tissue begins to heal[13] (subacute phase of myocardial infarction, MI) and spontaneous ventricular arrhythmias can take place in this period.[14,15] Finally, complete healing and scar formation occurs after several days (or weeks). In this chronic phase of MI, reentrant ventricular tachycardias (VTs) are still inducible, indicating that the arrhythmogenic substrate is still present, albeit the mechanisms of these chronic-phase arrhythmias are different from those of the acute phase.

Simulation of ischaemia and infarction

In the past decades, integrative computational simulation has become a powerful tool to complement experimental and clinical research when trying to elucidate the intimate mechanisms of ischaemic electrophysiological processes.[16-22] The heart is a particularly appropriate organ to be

computationally simulated on a multiscale basis because of the long history of cardiac cell modelling[23] and the continuous interaction between experiments and simulation. From the earliest Luo-Rudy models for guinea-pig ventricular cells[24] to the most recent electrophysiological model of human ventricular myocytes,[25] it has become possible to dynamically compute ionic currents through sarcolemmal channels and transporters, ion concentrations (including Ca^{2+} levels in the different subcellular compartments) and APs with great degree of electrophysiological detail. In parallel, medical imaging techniques have enabled us to reconstruct heart anatomy and structure "in silico", allowing multiscale computational simulations in which genetic defects, for instance, can be linked to the whole organ behaviour. These "virtual hearts" are today a perfect example of how an integrative biology approach may aid in the understanding of cardiac arrhythmias and in the improvement of therapeutic techniques such as drug administration, electrical defibrillation or radio-frequency ablation.

Acute myocardial ischaemia and MI are among the most successfully simulated cardiac pathologies.[17] Experimental understanding of the intimate mechanisms of acute ischaemia is particularly difficult due to the complex dynamics and unstable nature of the phenomenon, and the fact that most lethal arrhythmias occur before hospital admission makes it almost impossible to carry out systematic clinical studies. Also, the potential immediacy of death associated to ischaemic arrhythmias poses insurmountable ethical and practical obstacles. Therefore, computer simulations are of special importance. In the subacute and chronic stages of MI, simulations are also of great interest to aid the clinician during ablation interventions. This therapeutic procedure has unsatisfactory rates ranging 50% to 90%, and a consensus on the optimum approach does not exist.[26] Thus, multiscale image-based simulation is becoming a powerful tool which can provide guidance in defining the optimum ablation strategy.

Outline

The purpose of this paper is to briefly review some of the multiscale computational models of myocardial ischaemia and MI developed in the past twenty years. The review begins with a discussion of different models of acute ischaemia at the cellular level and then deals with the modelling of ischaemia-related tissue heterogeneities (i.e. the ischaemic border zone). Then, simulations of the electrical consequences of regional ischaemia (in the form of increased reentrant-type arrhythmia vulnerability) are discussed, both in phase 1A and phase 1B ischaemia. Next, models for the electrical and structural remodelling of infarcted tissue are presented. Finally, simulation of the electrical activity

in chronically infarcted tissue is discussed, including a very novel approach to myocardial ablation which uses image-based electrical simulations.

SIMULATION OF ISCHAEMIA AT THE CELLULAR LEVEL

It has been known for many years that acute ischaemia has three major components that result from cessation of blood flow: acidosis, hypoxia and hyperkalaemia.[27,28] Intracellular and extracellular pH values can drop from 7.2-7.4 to 6.2-6.4 in the first 10-20 minutes of ischaemia.[29] Oxygen deprivation provokes a moderate decline in ATP levels and an increase in ADP concentration in the intracellular medium.[30] Extracellular K^+ concentration ($[K^+]_o$) can increase more than two-fold in the first 10-15 minutes post occlusion before plateauing for another 15-20 minutes.[31-34] Each of these phenomena affects ion channels (and thereby APs) in a different manner[35] and ultimately set the stage for reentrant activity.[7]

Simulating acidosis in phase 1A ischaemia

In almost all ischaemic cellular models, the effects of acidosis are mimicked by reducing the maximum conductance of the fast Na^+ channels and the L-type Ca^{2+} channels.[36-38] A direct consequence of these changes is a reduction in cell excitability and upstroke velocity.[39,40] Very recently, Roberts and Christini included the Na^+/H^+ and other exchangers in the Luo-Rudy model[41] in order to analyse reperfusion arrhythmogenesis,[42] creating a new model which can accurately reproduce acidosis in acute ischaemia.

Simulating hypoxia in phase 1A ischaemia

Simulation of the electrophysiological effects of hypoxia has historically deserved much attention. The decline in ATP level reduces Na^+/K^+ pump (I_{NaK}) activity and activates the ATP-sensitive K^+ current ($I_{K(ATP)}$),[43] which is almost dormant in normoxic myocardium. To assess the electrophysiological effects of $I_{K(ATP)}$ activation, Ferrero *et al.*[44] proposed a model for $I_{K(ATP)}$ which included the modulation exerted by ATP and ADP,[30] intracellular Mg^{2+} and Na^+ [45] and $[K^+]_o$.[45] This model was incorporated into the Luo-Rudy ionic model[24,45] and APs were simulated under hypoxic conditions to try to elucidate the role of $I_{K(ATP)}$ activation in the well-known APD shortening in acute ischaemia.[47] The main results of the simulations, depicted in Figure 1A, showed that opening of very few (less than 1%) K_{ATP} channels may provoke a strong shortening in APD, with activation of only 0.6% of K_{ATP} channels needed to account for a 50% reduction in APD. These results confirmed the validity of the "spare channel hypothesis"[48] in the heart, something which was not completely clear in

view of some experimental results.[49] According to the results by Ferrero *et al.*, hyperkalaemia was only a secondary factor in explaining APD shortening during phase 1A ischaemia. Using a similar model for $I_{K(ATP)}$, Shaw and Rudy arrived to analogous results.[39,50]

Recently, a new and more comprehensive model for $I_{K(ATP)}$ was developed. Using new experimental data on Mg^{2+}, ATP and MgADP regulation of K_{ATP} channels and on the channel structure, Michailova *et al*.[51] reformulated the current and incorporated it to an ionic-metabolic model appropriate for excitation-metabolic coupling simulations under ischaemic conditions in the transmural ventricular wall.[52] The model was used to predict that K_{ATP} channels are activated transmurally with the smallest reduction in ATP in epicardial cells and largest in endocardial cells during phase 1A ischaemia and that inhomogeneous accumulation of metabolites in the transmural ventricular tissue may alter K_{ATP} channel opening in a very irregular manner, causing differential APD shortening across the ventricular wall.[52]

Simulating hyperkalaemia in phase 1A ischaemia

The causes and effects of hyperkalaemia have also deserved attention in computational simulation. Ischaemic elevation of $[K^+]_o$ forces cellular resting potential to become less negative (diastolic depolarization) and thus reduces cell excitability and delays its recovery (inducing post-repolarization refractoriness, PRR).[53] These effects of hyperkalaemia have been reproduced by simulating APs of single myocytes subject to acutely ischaemic conditions in isolated myocytes[39] and 1D strands.[50] Although these changes in cell excitability are strongly pro-arrhythmic because they promote unidirectional block (UDB) and reentry,[8,9,54,55] the intimate causes of cellular K^+ loss are still not well understood.

In 2002, Rodriguez *et al*.[56] used a single-cell model which dynamically calculated ion transfer and fluxes between three compartments (intracellular, interstitial cleft and bulk extracellular media) in ischaemic conditions. To simulate ionic currents and APs, the model used the Luo-Rudy membrane kinetics[24,46] including the formulation of $I_{K(ATP)}$ by Ferrero *et al*.[44] and an ischaemia-activated slow Na^+ current (I_{NaS}).[57] Figure 1B depicts the main results obtained with the model. According to the simulations, the concurrence of three mechanisms is needed to explain the biphasic time-course of $[K^+]_o$ in phase 1A ischaemia, namely $I_{K(ATP)}$ current activation,[58] I_{NaK} partial inhibition[59] and I_{NaS} activation.[57,58,60] The participation of only one or two of these mechanisms cannot explain the experimentally observed $[K^+]_o$ increase neither quantitatively nor qualitatively. Due to the non-linear

nature of the phenomenon, the algebraic addition of the separate effects of the three mechanisms (trace IV in Figure 1B) does not reproduce the time-course of $[K^+]_o$ either. However, if the three mechanisms take place simultaneously, the non-linear interactions between them increases the rate of $[K^+]_o$ rise, generates a plateau and the biphasic increase of $[K^+]_o$ can be nicely reproduced (trace VIII in Figure 1B). Interestingly, the quantitative contribution of $I_{K(ATP)}$ to the rise in $[K^+]_o$ is almost negligible (trace I), but its participation is essential to generate the plateau in $[K^+]_o$ (compare traces VII and VIII). The simulations also show that K^+ efflux mainly takes place through the time-independent K^+ channels (I_{K1}). Although these findings are difficult to be obtained using solely experimental means, further experiments should be undertaken in order to confirm the hypothesis suggested by the model.

Incorporating the effects of acidosis, hypoxia and hyperkalaemia into an AP model, the electrical activity of the phase 1A ischaemic cell can be computed and explained.[39,50] Figure 1C shows simulated APs of an isolated myocyte during four different stages of phase 1A ischaemia (0, 3, 7 and 11 minutes post occlusion, respectively).[56] The changes observed in APs are consistent with experimental findings.[30,32,35,61]

Simulating phase 1B ischaemia

In order to simulate phase 1B ischaemia, Pollard *et al.* proposed additional modifications in ionic currents and intracellular Ca^{2+} handling, including the acidotic inhibition of the Na^+/Ca^{2+} exchanger, an enhancement of the background Ca^{2+} current and the non-selective Ca^{2+}-sensitive cation current, and a reduction in the sarcoplasmic reticulum Ca^{2+} release current and the SERCA pump.[62]

THE BORDER ZONE IN ACUTE ISCHAEMIA

Modelling border zone gradients

In most cases, ischaemia is caused by the occlusion of a coronary artery and thus its nature is regional. A central ischemic zone (CIZ) is formed, constituted by cells directly affected by the lack of blood flow, while cells away from the CIZ are unaltered and form the normal zone (NZ). The transition between both zones is not abrupt but instead an ischaemic border zone (BZ) develops in which a gradient of ion and metabolite concentrations exists. This high degree of heterogeneity sets the stage for reentry.[63,64] The width of the BZ for each species is variable and has been characterized experimentally for some ions (particularly K^+)[65-68], but the profile and extension of the BZ for other species remains unclear.

Potse *et al*. used a one-dimensional (1D) diffusive model for K^+ ions to establish the spatial profile of $[K^+]_o$ across the BZ.[69] The results predict a non-linear $[K^+]_o$ spatial evolution within the BZ, showing a steep rise in the BZ adjacent to the NZ and a more flattened behaviour near the CIZ. The authors demonstrate that the diffusion constant which would be needed to explain the experimentally observed profile of K^+ in the BZ is too large, suggesting that physical diffusion is not the only mechanism that plays a role in the establishment of the BZ. Pulsative flow in the arterial and venous bed could be the other mechanism involved.[67]

More recently, Niederer extended the model to other species (Na^+, Ca^{2+}, Cl^- and H^+, among others).[70] An experimental measurement of the gradients of these ions in ischaemia is hampered by low spatial and/or temporal resolutions.[67,71] The model developed by Niederer is extremely comprehensive, as it includes dynamic descriptions of membrane kinetics, ionic currents, diffusive ion fluxes and Ca^{2+} regulation. The author was able to simulate the spatio-temporal profile of intracellular and extracellular concentrations. The results show that the ischaemic BZ is larger for extracellular K^+ (four times wider than the Na^+ BZ, for instance), which can be explained by the voltage-dependent nature of K^+ channels, and also that intracellular and extracellular K^+ concentrations may decrease within the CIZ due to electrogenic drift.

Simulating electrical activity in regional ischaemia

When the NZ, BZ and CIZ are included in a tissue model coupled to an ischaemic AP model, the electrical activity of an acutely ischaemic tissue can be simulated. Ferrero *et al.*[72] conducted simulations in an electrophysiologically detailed two-dimensional (2D) anisotropic tissue subject to 10-minutes of ischaemia. The tissue comprised a circular CIZ surrounded by a ring-shaped BZ with a width of 1 cm for $[K^+]_o$ and pH[65,73,74] and 1 mm for ATP/ADP,[74] enclosed in normal tissue (NZ). The results, shown in Figure 2, reveal profound electrophysiological changes within the BZ under normal pacing. First, CV slightly increases when entering the BZ (due to “supernormal conduction”),[50] but decreases in the second half of the BZ, plateauing at approximately 1/3 of its normal value in the CIZ due to the combined effects of hyperkalaemia and acidosis (see Figure 2A). Second, an sharp reduction in APD and effective refractory period (ERP) is found in the normal side of the BZ (due to abrupt $I_{K(ATP)}$ activation in the first millimetre of the BZ), but ERP subsequently increases across the BZ reaching almost normal values in the CIZ, mainly due to hyperkalaemia (Figure 2B). Thus, the model predicts a strong gradient in ERP across the BZ and a high degree of PRR (>80 ms) in the CIZ, which

is consistent with experimental findings by Zaitsev *et al*. in regionally ischaemic pig hearts.[64] Third, as shown in Figure 2C, acidosis and hyperkalaemia strongly reduce the inward Na^+ current (I_{Na}) peak in the CIZ, reaching a value comparable to the L-type Ca^{2+} current ($I_{Ca(L)}$) peak. This can be further appreciated in Figure 2D, where the time-course of AP, I_{Na} and $I_{Ca(L)}$ during the depolarization and early plateau phases is shown. The upstroke of the AP is divided into two distinct components (one supported by I_{Na} and the other by $I_{Ca(L)}$), something which has been observed experimentally.[7,53,75,76] The enhanced role of $I_{Ca(L)}$ in ischaemic propagation favours conduction block and the appearance of alternans, which in turn may provoke reentry as demonstrated also by Shaw and Rudy[40] and Bernus *et al.*[77] This highly heterogeneous substrate favours reentrant arrhythmias.

When phase 1B ischaemia is reached, the midmyocardial part of the CIZ becomes inexcitable,[78] acting as a partially depolarized sink. Viable cell layers survive in the subepicardium and the subendocardium, with ischaemic damage increasing over time.[79] Cellular uncoupling between the inexcitable midmyocardium and the survival layers begins to develop.[10] This substrate was modelled by Jie *et al.* to study phase 1B ischaemia arrhythmogenesis.[80,81]

VULNERABILITY TO REENTRY IN ISCHAEMIA

Using the same tissue model for phase 1A ischaemia described previously, Ferrero *et al.* studied the inducibility of reentry[72]. When paced at the same site as the basic beat, a premature stimulus could induce figure-of-eight reentrant patterns which nicely resembled those obtained experimentally.[8,9,63,82]

Similar reentrant patterns were obtained from simulations conducted in a three-dimensional (3D) reconstruction of the human ventricles with realistic anatomy and structure (obtained from diffusion tensor magnetic resonance imaging [DT-MRI]) and transmural heterogeneity (with different ionic computational models for epicardial, endocardial and midmyocardial cells).[83] Figure 3 shows the transmembrane potential distribution in selected instants just after the delivery of a premature stimulus in the subendocardial BZ, where premature excitations (the trigger for arrhythmia induction) normally originate.[8,35,73,76] An arc of functional conduction block develops in the innermost side of the BZ (third snapshot), caused by the prolonged refractoriness of the tissue (PRR is near its maximum at that site), giving rise to UDB and figure-of-eight reentry.[84]

The time-course of arrhythmia vulnerability

According to different experimental and clinical observations, the likelihood of arrhythmic events reaches a maximum before the 10th minute, decreases again giving rise to an arrhythmias-scarce period at the end of phase 1A, and increases subsequently in phase 1B.[11,12,85] The reasons for this triphasic behaviour are still not completely established. Using the same 2D model described above, Trenor *et al.* studied the time-evolution of reentry inducibility during the first 10 minutes of ischaemia.[86] The authors quantified the "vulnerable window" (VW, defined as the time interval during which a premature stimulus - delivered after a conditioning stimulus - triggers reentry) at selected time points post occlusion. The results were consistent with experimental observations: the VW begins to increase 6.5 minutes after the onset of ischaemia, peaks at the 8th minute and vanishes in the 9th minute. According to the simulation results, reentry needs the combination of severe hyperkalaemia with moderate hypoxia and acidosis to occur, and those conditions are met in the third quarter (minutes 5 to 7.5) of phase 1A ischaemia. Severe hyperkalaemia ($[K^+]_o$>12 mmol/L) is needed to generate enough PRR to create an arc of block, while strong acidosis (weak I_{Na} and $I_{Ca(L)}$) and/or hypoxia (strong $I_{K(ATP)}$) would in turn block retrograde propagation in the CIZ creating a BDB that prevents reentry.[86]

Using the same AP and tissue and model, the same group conducted simulations to assess the proarrhythmic or antiarrhythmic effects of two well-known drugs. According to their simulation results, pinacidil[87] was shown to be proarrhythmic (incrementing the VW) at low concentrations but protective at concentrations higher than 10 μmol/L,[88] while lidocaine[89] facilitates the onset of reentry in ischaemic ventricular tissue.[90]

In a similar study using a 2D slice of virtual acutely ischaemic ventricular tissue, Tice *et al.* highlighted the importance of transmural heterogeneity in the development of phase 1A arrhythmias.[4] Experimental studies usually focus on epicardial manifestations of arrhythmias due to logical limitations related to the penetration depth of optical mapping techniques. In their simulation study, three BZs (lateral, endocardial and epicardial) of different widths were defined, and transmural heterogeneities in the ischaemic severity were included (with $[K^+]_o$ rising at a faster rate in the subendocardium and hypoxia affecting more severely in the subepicardium). Their results suggest that transmural gradients of $I_{K(ATP)}$ activation strongly increase arrhythmogenesis, with almost no sustained reentrant activity observed in the absence of $I_{K(ATP)}$ heterogeneity. Reentrant likelihood also peaked in

the 8th minute post occlusion. The importance of transmural ischaemic heterogeneity was also stressed in the work by Weiss *et al.* which used a 3D model of the human ventricles.[91]

Dispersion of refractoriness and arrhythmia vulnerability

According to different experimental[64,68,92] and theoretical[93,94] studies, spatial dispersion of repolarization and/or refractoriness increases reentry vulnerability. Romero *et al.* used a 2D ventricular model developed by Ferrero *et al.* [72,86] to test this hypothesis in the case of phase 1A ischaemia.[95] According to their results, summarized in Figure 4, ERP dispersion and arrhythmia vulnerability only correlate well in the first 8 minutes of ischaemia but diverge in the last part of phase 1A, when arrhythmias cease to occur but ERP dispersion keeps increasing. According to their results, UDB took place in cells completely recovered from refractoriness in almost 50% of reentries. The authors argue that local source-sink relationship determines the formation of UDB, and propose a modified version of the safety factor (which quantifies the sink-source mismatch in the propagation process)[96,97] as a better tool to analyse the causes of UDB in ischaemia.

The role of mechanoelectrical feedback

In all the simulations mentioned above, the trigger for reentry was artificially applied in the form of a premature stimulus externally delivered at a certain site (normally the subendocardial BZ)[8,73,76], so no inference can be made about the originating mechanism of reentry. Recent multiscale simulations by Jie *et al.* suggest that mechanoelectrical feedback may play a pivotal role.[98] The simulations involved 3D anatomically and structurally accurate virtual rabbit ventricles in which occlusion of the LAD artery was simulated. The ionic model employed included a mathematical description of two distinct mechanosensitive channels,[99] and it also included a novel bidomain electro-mechanical model. According to their results, mechanosensitive ionic channels[100] are recruited due to the non-uniformity of mechanical strain during acutely ischaemic contractions, resulting in suprathreshold depolarizations in the BZ which act as the trigger of the premature beat that, in turn, elicits reentry. Additionally, delayed after-depolarizations (DAD) also resulting from mechanoelectrical feedback in the ischaemic region can contribute to lower excitability, enhancing refractoriness in the CIZ and favouring reentry.

Arrhythmias in phase 1B ischaemia

Less attention has been paid to the mechanisms of arrhythmias in phase 1B ischaemia. In 2003, Pollard *et al.* conducted simulations in a 1D strand comprising 1 cm of normal tissue coupled to

1 cm of cells affected by phase 1B ischaemia.[101] The results indicated that suprathreshold DADs develop in the ischaemic zone and only propagate to normal tissue in the form of APs when intermediate uncoupling between the two zones is present. The fact that moderate uncoupling is an important contributor to phase 1B arrhythmogenesis was further stressed by the work of Jie *et al.*[80] in which they coupled an inexcitable midmyocardial zone to a surviving subepicardial layer via a thin coupling layer. The results suggested that heterogeneous uncoupling between layers enhance ERP dispersion in the subepicardium, thus increasing reentry vulnerability. Complete uncoupling eliminated arrhythmias. In a more recent work, Jie and Trayanova improved the model by using 3D rabbit ventricle geometry and simulating a more complex substrate structure which comprised a CIZ with inexcitable midmyocardium and surviving subepicardial and subendocardial layers, as well as lateral BZs.[81] According to their results, the degree of hyperkalaemia in the subepicardium was key, as it led to the induction of reentrant activity. Vulnerability to reentry was biphasic, with increased cellular uncoupling and reduction of the width of the lateral BZ increasing reentry inducibility.

Simulating global ischaemia

When ischaemia results from a coronary artery occlusion, it is regional by nature, but during ventricular fibrillation (VF) ischaemia becomes global as perfusion of the myocardium is interrupted. However, simulation works dealing with global ischaemia are not as abundant as those that model regional ischaemia. Among them, a recent paper[102] simulates global ischaemia in a 2D virtual tissue to provide some insights into the effects of ischaemia on the organization of VF. With a different aim, Rodriguez *et al.* simulated global ischaemia in a 2D slice of myocardium[103] and in 3D rabbit ventricles[104] to study the effects of phase 1A global ischaemia on the upper limit of vulnerability to electric shocks in the context of electrical defibrillation.

ELECTRICAL AND STRUCTURAL REMODELLING IN INFARCTED TISSUE

Three to five days after the initial ischaemic event, electrical[13,14] and structural[13] remodelling of the epicardial BZ (EBZ) begins. These changes in the substrate can eventually generate arrhythmias in the subacute and chronic phases of MI[105] and have received attention in the past 10 years from the computational simulation community.

Electrical remodelling

Within the EBZ, experimental studies have recorded shorter,[13] similar[13,106] or longer[107] APD than in normal myocardium. However, the EBZ has a longer refractory period due to the existence of

PRR.[14,108] Using experimental data from remodelled ionic currents, Cabo and Boyden formulated a computational model for EBZ cells.[109] They modified the Luo-Rudy model to include alterations in the maximal conductance and kinetics of I_{Na},[106] $I_{Ca(L)}$,[110] I_{Kr},[111] I_{Ks},[112] and $I_{K1.}$[112] More recently, Decker and Rudy[113] developed a new model of the remodelled EBZ by additionally altering the maximum conductance and kinetics of I_{to2}[114] and I_{to1}.[106] Applying these modifications to the basic Luo-Rudy model, the authors were able to reproduce the aforementioned features of APs of cells in the EBZ. Even more recently, McDowell *et al.* adapted a rabbit AP model in the same direction.[115]

Structural remodelling

In reference to structural remodelling, gap junctional changes and fibrotic remodelling have been observed in post-infarcted hearts[112,113] with conduction disturbances observed in the healing infarct BZ being related to intercellular uncoupling.[117,118] Marked alterations in the organization of intercellular connections occur in the EBZ, leading to non-uniform conduction, fractionated electrograms and reentry.[118] Several theoretical investigations using computer simulations have addressed the role of altered cellular coupling on AP conduction.[119,120] Cellular uncoupling not only decreases conduction velocity, but it may create a substrate that facilitates the propagation of ectopic activity.[121,122] It is thus an important factor to consider when implementing realistic electrical models of the infarcted heart in the subacute and chronic phases.

Experimental evidence exists according to which myofibroblasts proliferate following myocardial infarction, especially in the peri-infarct zone.[123,124] Electrical coupling between myofibroblasts and myocytes is well established in cell culture[125] and the presence of fibrotic areas in the ventricle leads to altered and discontinuous conduction and fractionated electrograms.[126,127] Several theoretical studies focusing on the electrotonic coupling between fibroblasts and myocytes use computational models of the passive and active electrical behaviour of fibroblasts.[128-130] Simulations reveal significant electrophysiological consequences of coupling fibroblasts to myocytes at the cellular level, such as partial diastolic depolarization of the myocyte and significant shortening of its APD.[128] Also, the critical pacing cycle length at which alternans occur is changed by fibroblast-myocyte coupling.[131] In results obtained from 1D and 2D simulations, conduction disturbances arise in the presence of fibrosis[132,133] and changes in electrical restitution properties occur, leading to spiral wave instability.[134,135] Using 2D simulations, Xie *et al.* observed an increased vulnerability to reentry in

the presence of fibrosis.[131] Fractionated electrograms were also obtained in 2D simulated ventricular tissues with different fibrosis densities.[136]

SIMULATION OF MYOCARDIAL INFARCTION AT THE ORGAN LEVEL

Three-dimensional ventricular simulations including fibrosis are very recent. McDowell *et al.* simulated the electrical activity of anatomically realistic rabbit ventricles in the presence of an infarction scar, a remodelled peri-infarct zone and different levels of fibrosis.[115] The authors observed an increase in the vulnerability to reentry in the presence of intermediate fibrosis, while high densities of fibroblasts reduced the probability of reentry. To run the simulations, they developed a 3D computational model of the chronically infarcted rabbit ventricles based on MRI. Recent advances in MRI technologies have facilitated the imaging of geometry and tissue architecture at improved resolution, so image-based methods have been recently developed to construct computational models,[137] and many of them focus on the arrhythmogenic behaviour of the infarcted heart.

Rantner *et al.* analysed the mechanisms of decreased defibrillation efficacy in infarcted hearts using an improved model of the rabbit infarcted ventricle.[138] Vigmond *et al.* analysed reentrant mechanisms in a canine infarction 3D model also using image-based modelling techniques.[139] Their model included a scar and the BZ with electrical remodelling. Swine models of myocardial infarction have also been reconstructed based on MRI.[140-142] Pop *et al.*[140] showed that computer simulation based on ex-vivo DT-MRI could predict the VT circuit obtained in swine electrophysiological studies. Their 3D model included healthy tissue, scar and BZ using a two-variable model of the AP. Similarly, Ng *et al.*[142] included electrically remodelled grey zones and infarct cores in swine hearts. VT was induced in different virtual models and showed that a combination of infarct scars and peri-infarct zones is needed for VT generation. Similar reentrant circuits were obtained in the electrophysiological studies and in the virtual ones, demonstrating that image-based modelling may be helpful when planning catheter ablation strategies. Indeed, very recently, Ashikaga *et al.* tested the feasibility of image-based simulation to estimate ablation targets in human VT, highlighting the effectiveness of this non-invasive tool.[143] As shown in Figure 5, their model includes infarct zones, grey zones with electrical remodelling, and healthy zones. When ablation in the human patient was done within the zone predicted by the model, successful termination of reentry was accomplished. This model is state-of-the-art in image-based simulation oriented to ablation strategy optimization.

SUMMARY

This article provided a brief review of some of the multiscale computational models of myocardial ischaemia and MI developed in the past years. The models discussed here are examples of how computer simulations may help to understand the electrical consequences of ischaemia and MI and to improve treatments of subsequent cardiac arrhythmias. At the cellular level, simulations have contributed to elucidate the ionic mechanisms responsible for the ischaemia-induced changes in APs and ionic concentrations and have aided in better understanding how the ischaemic border zone is established. Regarding ischaemic arrhythmogenesis, the models have helped to clarify the role of acidosis, hypoxia and hyperkalaemia in the onset and maintenance of ischaemic reentry and to theoretically explain the biphasic nature of arrhythmia vulnerability in phase 1A ischaemia. Simulations have also shed new light on the role of dispersion of refractoriness, source-sink mismatch and mechanoelectrical feedback in arrhythmogenesis.

Today, computational simulations are also helping to improve therapeutic techniques to stop and/or prevent arrhythmias in ischaemic patients. Modelling the interaction between different drugs (such as lidocaine or pinacidil) and their molecular targets has enabled us to explain (and, ideally, predict) the proarrhythmic or antiarrhythmic effects of these drugs in an ischaemic scenario. Also, recent works are beginning to show how computer simulations can be useful to improve electrical arrhythmia treatment.

In the task of integrating computer simulation techniques in daily clinical practice in the context of ischaemia and MI, important limitations are yet to be addressed. At the cellular level, ionic models need to be improved using new patch-clamp data from human ischaemic hearts. At the tissue level, it is still impossible to visualize the actual fibre orientation of the in-vivo infarcted heart of a patient. When these and other limitations are overcome, the use of computational simulations to optimize myocardial ablation procedures in infarcted patients,[143] for instance, will become a real possibility.

FUNDING

This work was partially supported by the “VI Plan Nacional de Investigación Científica, Desarrollo e Innovación Tecnológica” from the Ministerio de Economía y Competitividad of Spain (grant number TIN2012-37546-C03-01) and the European Commission (European Regional

Development Funds – ERDF - FEDER), and by the Dirección General de Política Científica de la Generalitat Valenciana (grant number GV/2013/119).

5

References

1. Steg PG, James SK, Atar D, Badano LP, Blomstrom-Lundqvist C, Borger MA, et al. ESC Guidelines for the management of acute myocardial infarction in patients presenting with ST-segment elevation. *Eur Heart J* 2012 Oct;**33**(20):2569-619.

2. Roger VL, Go AS, Lloyd-Jones DM, Benjamin EJ, Berry JD, Borden WB, et al. Heart disease and stroke statistics--2012 update: a report from the American Heart Association. *Circulation* 2012 Jan 3;**125**(1):e2-e220.

3. Zipes DP, Wellens HJ. Sudden cardiac death. *Circulation* 1998 Nov 24;**98**(21):2334-51.

4. Goldberger JJ, Cain ME, Hohnloser SH, Kadish AH, Knight BP, Lauer MS, et al. American Heart Association/American College of Cardiology Foundation/Heart Rhythm Society scientific statement on noninvasive risk stratification techniques for identifying patients at risk for sudden cardiac death: a scientific statement from the American Heart Association Council on Clinical Cardiology Committee on Electrocardiography and Arrhythmias and Council on Epidemiology and Prevention. *Circulation* 2008 Sep 30;**118**(14):1497-518.

5. Rubart M, Zipes DP. Mechanisms of sudden cardiac death. *J Clin Invest* 2005 Sep;**115**(9):2305-15.

6. Ferrero JM, Ferrero A, Trenor B, Montilla F, Saiz J, Rodriguez B. Ischemia. In: Akay M, ed. *Wiley Encyclopedia of Biomedical Engineering*. John Wiley and Sons 2006.

7. Wit AL, Janse MJ. The ventricular arrhythmias of ischemia and infarction: electrophysiological mechanisms. Futura Publishing Co. ed. Mount Kisko: 1993.

8. Janse MJ, van Capelle FJ, Morsink H, Kleber AG, Wilms-Schopman F, Cardinal R, et al. Flow of "injury" current and patterns of excitation during early ventricular arrhythmias in acute

regional myocardial ischemia in isolated porcine and canine hearts. Evidence for two different arrhythmogenic mechanisms. *Circ Res* 1980 Aug;**47**(2):151-65.

9. Janse MJ, Kleber AG. Electrophysiological changes and ventricular arrhythmias in the early phase of regional myocardial ischemia. *Circ Res* 1981 Nov;**49**(5):1069-81.

10. de Groot JR, Wilms-Schopman FJ, Opthof T, Remme CA, Coronel R. Late ventricular arrhythmias during acute regional ischemia in the isolated blood perfused pig heart. Role of electrical cellular coupling. *Cardiovasc Res* 2001 May;**50**(2):362-72.

11. Kaplinsky E, Ogawa S, Balke CW, Dreifus LS. Two periods of early ventricular arrhythmia in the canine acute myocardial infarction model. *Circulation* 1979 Aug;**60**(2):397-403.

12. Smith WT, Fleet WF, Johnson TA, Engle CL, Cascio WE. The Ib phase of ventricular arrhythmias in ischemic in situ porcine heart is related to changes in cell-to-cell electrical coupling. Experimental Cardiology Group, University of North Carolina. *Circulation* 1995 Nov 15;**92**(10):3051-60.

13. Ursell PC, Gardner PI, Albala A, Fenoglio JJ, Jr., Wit AL. Structural and electrophysiological changes in the epicardial border zone of canine myocardial infarcts during infarct healing. *Circ Res* 1985 Mar;**56**(3):436-51.

14. Lazzara R, Scherlag BJ. Electrophysiologic basis for arrhythmias in ischemic heart disease. *Am J Cardiol* 1984 Feb 27;**53**(5):1B-7B.

15. Pantridge JF, Webb SW, Adgey AA. Arrhythmias in the first hours of acute myocardial infarction. *Prog Cardiovasc Dis* 1981 Jan;**23**(4):265-78.

16. Noble D. Modeling the heart--from genes to cells to the whole organ. *Science* 2002 Mar 1;**295**(5560):1678-82.

17. Rodriguez B, Trayanova N, Noble D. Modeling cardiac ischemia. *Ann N Y Acad Sci* 2006 Oct;**1080**:395-414.

18. Trayanova NA, Tice BM. Integrative computational models of cardiac arrhythmias -- simulating the structurally realistic heart. *Drug Discov Today Dis Models* 2009;**6**(3):85-91.

19. Silva JR, Rudy Y. Multi-scale electrophysiology modeling: from atom to organ. *J Gen Physiol* 2010 Jun;**135**(6):575-81.

20. Trayanova NA. Whole-heart modeling: applications to cardiac electrophysiology and electromechanics. *Circ Res* 2011 Jan 7;**108**(1):113-28.

21. Trenor Gomis B, Romero L, Cardona K, Gomis-Tena J, Saiz J, Ferrero (Jr) JM. Multiscale Modeling of Myocardial Electrical Activity: From Cell to Organ. *Biomedical Engineering*. 2011: 337-60.

22. Trayanova NA, O'Hara T, Bayer JD, Boyle PM, McDowell KS, Constantino J, et al. Computational cardiology: how computer simulations could be used to develop new therapies and advance existing ones. *Europace* 2012 Nov;**14 Suppl 5**:v82-v89.

23. Noble D. Cardiac action and pacemaker potentials based on the Hodgkin-Huxley equations. *Nature* 1960 Nov 5;**188**:495-7.

24. Luo CH, Rudy Y. A dynamic model of the cardiac ventricular action potential. I. Simulations of ionic currents and concentration changes. *Circ Res* 1994 Jun;**74**(6):1071-96.

25. O'Hara T, Virag L, Varro A, Rudy Y. Simulation of the undiseased human cardiac ventricular action potential: model formulation and experimental validation. *PLoS Comput Biol* 2011 May;**7**(5):e1002061.

26. Aliot EM, Stevenson WG, Almendral-Garrote JM, Bogun F, Calkins CH, Delacretaz E, et al. EHRA/HRS Expert Consensus on Catheter Ablation of Ventricular Arrhythmias: developed in a partnership with the European Heart Rhythm Association (EHRA), a Registered Branch of the European Society of Cardiology (ESC), and the Heart Rhythm Society (HRS); in collaboration with the American College of Cardiology (ACC) and the American Heart Association (AHA). *Europace* 2009 Jun;**11**(6):771-817.

27. Morena H, Janse MJ, Fiolet JW, Krieger WJ, Crijns H, Durrer D. Comparison of the effects of regional ischemia, hypoxia, hyperkalemia, and acidosis on intracellular and extracellular potentials and metabolism in the isolated porcine heart. *Circ Res* 1980 May;**46**(5):634-46.

28. Kodama I, Wilde A, Janse MJ, Durrer D, Yamada K. Combined effects of hypoxia, hyperkalemia and acidosis on membrane action potential and excitability of guinea-pig ventricular muscle. *J Mol Cell Cardiol* 1984 Mar;**16**(3):247-59.

29. Marban E, Kitakaze M, Koretsune Y, Yue DT, Chacko VP, Pike MM. Quantification of [Ca2+]i in perfused hearts. Critical evaluation of the 5F-BAPTA and nuclear magnetic resonance method as applied to the study of ischemia and reperfusion. *Circ Res* 1990 May;**66**(5):1255-67.

30. Weiss JN, Venkatesh N, Lamp ST. ATP-sensitive K+ channels and cellular K+ loss in hypoxic and ischaemic mammalian ventricle. *J Physiol* 1992 Feb;**447**:649-73.

31. Gasser RN, Vaughan-Jones RD. Mechanism of potassium efflux and action potential shortening during ischaemia in isolated mammalian cardiac muscle. *J Physiol* 1990 Dec;**431**:713-41.

32. Weiss J, Shine KI. [K+]o accumulation and electrophysiological alterations during early myocardial ischemia. *Am J Physiol* 1982 Aug;**243**(2):H318-H327.

33. Weiss J, Shine KI. Effects of heart rate on extracellular [K+] accumulation during myocardial ischemia. *Am J Physiol* 1986 Jun;**250**(6 Pt 2):H982-H991.

34. Yan GX, Chen J, Yamada KA, Kleber AG, Corr PB. Contribution of shrinkage of extracellular space to extracellular K+ accumulation in myocardial ischaemia of the rabbit. *J Physiol* 1996 Jan 1;**490 (Pt 1)**:215-28.

35. Carmeliet E. Cardiac ionic currents and acute ischemia: from channels to arrhythmias. *Physiol Rev* 1999 Jul;**79**(3):917-1017.

36. Kagiyama Y, Hill JL, Gettes LS. Interaction of acidosis and increased extracellular potassium on action potential characteristics and conduction in guinea pig ventricular muscle. *Circ Res* 1982 Nov;**51**(5):614-23.

37. Sato R, Noma A, Kurachi Y, Irisawa H. Effects of intracellular acidification on membrane currents in ventricular cells of the guinea pig. *Circ Res* 1985 Oct;**57**(4):553-61.

38. Irisawa H, Sato R. Intra- and extracellular actions of proton on the calcium current of isolated guinea pig ventricular cells. *Circ Res* 1986 Sep;**59**(3):348-55.

39. Shaw RM, Rudy Y. Electrophysiologic effects of acute myocardial ischemia: a theoretical study of altered cell excitability and action potential duration. *Cardiovasc Res* 1997 Aug;**35**(2):256-72.

40. Shaw RM, Rudy Y. Ionic mechanisms of propagation in cardiac tissue. Roles of the sodium and L-type calcium currents during reduced excitability and decreased gap junction coupling. *Circ Res* 1997 Nov;**81**(5):727-41.

41. Hund TJ, Kucera JP, Otani NF, Rudy Y. Ionic charge conservation and long-term steady state in the Luo-Rudy dynamic cell model. *Biophys J* 2001 Dec;**81**(6):3324-31.

42. Roberts BN, Christini DJ. NHE inhibition does not improve Na(+) or Ca(2+) overload during reperfusion: using modeling to illuminate the mechanisms underlying a therapeutic failure. *PLoS Comput Biol* 2011 Oct;**7**(10):e1002241.

43. Noma A. ATP-regulated K+ channels in cardiac muscle. *Nature* 1983 Sep 8;**305**(5930):147-8.

44. Ferrero JM, Jr., Saiz J, Ferrero JM, Thakor NV. Simulation of action potentials from metabolically impaired cardiac myocytes. Role of ATP-sensitive K+ current. *Circ Res* 1996 Aug;**79**(2):208-21.

45. Horie M, Irisawa H, Noma A. Voltage-dependent magnesium block of adenosine-triphosphate-sensitive potassium channel in guinea-pig ventricular cells. *J Physiol* 1987 Jun;**387**:251-72.

46. Zeng J, Laurita KR, Rosenbaum DS, Rudy Y. Two components of the delayed rectifier K+ current in ventricular myocytes of the guinea pig type. Theoretical formulation and their role in repolarization. *Circ Res* 1995 Jul;**77**(1):140-52.

47. Trautwein W, Gottstein U, Dudel J. The action current of the myocardial fibers in oxygen deficiency. *Pflugers Arch* 1954;**260**(1):40-60.

48. Cook DL, Satin LS, Ashford ML, Hales CN. ATP-sensitive K+ channels in pancreatic beta-cells. Spare-channel hypothesis. *Diabetes* 1988 May;**37**(5):495-8.

49. Yan GX, Yamada KA, Kleber AG, McHowat J, Corr PB. Dissociation between cellular K+ loss, reduction in repolarization time, and tissue ATP levels during myocardial hypoxia and ischemia. *Circ Res* 1993 Mar;**72**(3):560-70.

50. Shaw RM, Rudy Y. Electrophysiologic effects of acute myocardial ischemia. A mechanistic investigation of action potential conduction and conduction failure. *Circ Res* 1997 Jan;**80**(1):124-38.

51. Michailova A, Saucerman J, Belik ME, McCulloch AD. Modeling regulation of cardiac KATP and L-type Ca2+ currents by ATP, ADP, and Mg2+. *Biophys J* 2005 Mar;**88**(3):2234-49.

52. Michailova A, Lorentz W, McCulloch A. Modeling transmural heterogeneity of K(ATP) current in rabbit ventricular myocytes. *Am J Physiol Cell Physiol* 2007 Aug;**293**(2):C542-C557.

53. Downar E, Janse MJ, Durrer D. The effect of "ischemic" blood on transmembrane potentials of normal porcine ventricular myocardium. *Circulation* 1977 Mar;**55**(3):455-62.

54. Harris AS, Bisteni A, Russell RA, Brigham JC, Firestone JE. Excitatory factors in ventricular tachycardia resulting from myocardial ischemia; potassium a major excitant. *Science* 1954 Feb 12;**119**(3085):200-3.

55. Kleber AG. Conduction of the impulse in the ischemic myocardium--implications for malignant ventricular arrhythmias. *Experientia* 1987 Oct 15;**43**(10):1056-61.

56. Rodriguez B, Ferrero JM, Jr., Trenor B. Mechanistic investigation of extracellular K+ accumulation during acute myocardial ischemia: a simulation study. *Am J Physiol Heart Circ Physiol* 2002 Aug;**283**(2):H490-H500.

57. Ju YK, Saint DA, Gage PW. Hypoxia increases persistent sodium current in rat ventricular myocytes. *J Physiol* 1996 Dec 1;**497 (Pt 2)**:337-47.

58. Wilde AA, Aksnes G. Myocardial potassium loss and cell depolarisation in ischaemia and hypoxia. *Cardiovasc Res* 1995 Jan;**29**(1):1-15.

59. Wilde AA, Peters RJ, Janse MJ. Catecholamine release and potassium accumulation in the isolated globally ischemic rabbit heart. *J Mol Cell Cardiol* 1988 Oct;**20**(10):887-96.

60. Shivkumar K, Deutsch NA, Lamp ST, Khuu K, Goldhaber JI, Weiss JN. Mechanism of hypoxic K loss in rabbit ventricle. *J Clin Invest* 1997 Oct 1;**100**(7):1782-8.

61. Kleber AG, Riegger CB, Janse MJ. Extracellular K+ and H+ shifts in early ischemia: mechanisms and relation to changes in impulse propagation. *J Mol Cell Cardiol* 1987 Oct;**19 Suppl 5**:35-44.

62. Pollard AE. From myocardial cell models to action potential propagation. *J Electrocardiol* 2003;**36 Suppl**:43-9.

63. Kleber AG. Conduction of the impulse in the ischemic myocardium--implications for malignant ventricular arrhythmias. *Experientia* 1987 Oct 15;**43**(10):1056-61.

64. Zaitsev AV, Guha PK, Sarmast F, Kolli A, Berenfeld O, Pertsov AM, et al. Wavebreak formation during ventricular fibrillation in the isolated, regionally ischemic pig heart. *Circ Res* 2003 Mar;**92**(5):546-53.

65. Janse MJ, Cinca J, Morena H, Fiolet JW, Kleber AG, de Vries GP, et al. The "border zone" in myocardial ischemia. An electrophysiological, metabolic, and histochemical correlation in the pig heart. *Circ Res* 1979 Apr;**44**(4):576-88.

66. Walfridsson H, Odman S, Lund N. Myocardial oxygen pressure across the lateral border zone after acute coronary occlusion in the pig heart. *Adv Exp Med Biol* 1985;**191**:203-10.

67. Coronel R, Fiolet JW, Wilms-Schopman FJ, Schaapherder AF, Johnson TA, Gettes LS, et al. Distribution of extracellular potassium and its relation to electrophysiologic changes during acute myocardial ischemia in the isolated perfused porcine heart. *Circulation* 1988 May;**77**(5):1125-38.

68. Coronel R. Heterogeneity in extracellular potassium concentration during early myocardial ischaemia and reperfusion: implications for arrhythmogenesis. *Cardiovasc Res* 1994 Jun;**28**(6):770-7.

69. Potse M, Coronel R, LeBlanc AR, Vinet A. The role of extracellular potassium transport in computer models of the ischemic zone. *Med Biol Eng Comput* 2007 Dec;**45**(12):1187-99.

70. Niederer S. Regulation of ion gradients across myocardial ischemic border zones: a biophysical modelling analysis. *PLoS One* 2013;**8**(4):e60323.

71. Wilensky RL, Tranum-Jensen J, Coronel R, Wilde AA, Fiolet JW, Janse MJ. The subendocardial border zone during acute ischemia of the rabbit heart: an electrophysiologic, metabolic, and morphologic correlative study. *Circulation* 1986 Nov;**74**(5):1137-46.

72. Ferrero Jr JM, Trenor B, Rodriguez B, Saiz J. Electrical activity and reentry during acute regional myocardial ischemia: insights from simulations. *Int J Bif Chaos* 2003 Dic;**13**(12):3703-15.

73. Coronel R, Fiolet JW, Wilms-Schopman FJ, Schaapherder AF, Johnson TA, Gettes LS, et al. Distribution of extracellular potassium and its relation to electrophysiologic changes during acute myocardial ischemia in the isolated perfused porcine heart. *Circulation* 1988 May;**77**(5):1125-38.

74. Coronel R. Distribution of extracellular potassium during myocardial ischemia [Ph.D. thesis] University of Amsterdam; 1988.

75. Kleber AG, Janse MJ, van Capelle FJ, Durrer D. Mechanism and time course of S-T and T-Q segment changes during acute regional myocardial ischemia in the pig heart determined by extracellular and intracellular recordings. *Circ Res* 1978 May;**42**(5):603-13.

76. Pogwizd SM, Corr PB. Electrophysiologic mechanisms underlying arrhythmias due to reperfusion of ischemic myocardium. *Circulation* 1987 Aug;**76**(2):404-26.

77. Bernus O, Zemlin CW, Zaritsky RM, Mironov SF, Pertsov AM. Alternating conduction in the ischaemic border zone as precursor of reentrant arrhythmias: A simulation study. *Europace* 2005 Sep;**7**:S93-S104.

78. Kimura S, Bassett AL, Gaide MS, Kozlovskis PL, Myerburg RJ. Regional changes in intracellular potassium and sodium activity after healing of experimental myocardial infarction in cats. *Circ Res* 1986 Feb;**58**(2):202-8.

79. Fujiwara H, Ashraf M, Sato S, Millard RW. Transmural cellular damage and blood flow distribution in early ischemia in pig hearts. *Circ Res* 1982 Dec;**51**(6):683-93.

80. Jie X, Rodriguez B, de Groot JR, Coronel R, Trayanova N. Reentry in survived subepicardium coupled to depolarized and inexcitable midmyocardium: insights into arrhythmogenesis in ischemia phase 1B. *Heart Rhythm* 2008 Jul;**5**(7):1036-44.

81. Jie X, Trayanova NA. Mechanisms for initiation of reentry in acute regional ischemia phase 1B. *Heart Rhythm* 2010 Mar;**7**(3):379-86.

82. Costeas C, Peters NS, Waldecker B, Ciaccio EJ, Wit AL, Coromilas J. Mechanisms causing sustained ventricular tachycardia with multiple QRS morphologies: results of mapping studies in the infarcted canine heart. *Circulation* 1997 Nov 18;**96**(10):3721-31.

83. Heidenreich E, Ferrero JM, Rodriguez JF. Modeling the Human Heart Under Acute Ischemia. In: Calbo E, Peña B, eds. *Patient-Specific Computational Modeling*. Springer 2012.

84. Heidenreich E. Algorithms for reaction-diffusion equations applied to electrophysiology [Ph.D. thesis] University of Zaragoza; 2009.

85. de Groot JR, Coronel R. Acute ischemia-induced gap junctional uncoupling and arrhythmogenesis. *Cardiovasc Res* 2004 May 1;**62**(2):323-34.

86. Trenor B, Romero L, Ferrero JM, Jr., Saiz J, Molto G, Alonso JM. Vulnerability to Reentry in a Regionally Ischemic Tissue: A Simulation Study. *Ann Biomed Eng* 2007 Jul 7;**35**(10):1756-70.

87. Fan Z, Nakayama K, Hiraoka M. Multiple actions of pinacidil on adenosine triphosphate-sensitive potassium channels in guinea-pig ventricular myocytes. *J Physiol* 1990 Nov;**430**:273-95.

88. Trenor B, Ferrero JM, Jr., Rodriguez B, Montilla F. Effects of pinacidil on reentrant arrhythmias generated during acute regional ischemia: a simulation study. *Ann Biomed Eng* 2005 Jul;**33**(7):897-906.

89. Clarkson CW, Matsubara T, Hondeghem LM. Evidence for voltage-dependent block of cardiac sodium channels by tetrodotoxin. *J Mol Cell Cardiol* 1988 Dec;**20**(12):1119-31.

90. Cardona K, Trenor B, Molto G, Martinez M, Ferrero JM, Jr., Starmer F, et al. Exploring the role of pH in modulating the effects of lidocaine in virtual ischemic tissue. *Am J Physiol Heart Circ Physiol* 2010 Nov;**299**(5):H1615-H1624.

91. Weiss DL, Ifland M, Sachse FB, Seemann G, Dossel O. Modeling of cardiac ischemia in human myocytes and tissue including spatiotemporal electrophysiological variations. *Biomed Tech (Berl)* 2009 Jun;**54**(3):107-25.

92. Kuo C-S, Reddy CP, Munakata K, Surawicz B. Arrhythmias dependent predominantly on dispersion of repolarization. *Cardiac Electrphysiology and Arrhythmias*. 1985: 277-85.

93. Moe GK, Rheinboldt WC, Abildskov JA. A computer model of atrial fibrillation. *Am Heart J* 1964 Feb;**67**:200-20.

94. Clayton RH, Holden AV. Dispersion of cardiac action potential duration and the initiation of re-entry: a computational study. *Biomed Eng Online* 2005;**4**(1):11.

95. Romero L, Trenor B, Alonso JM, Tobon C, Saiz J, Ferrero JM, Jr. The relative role of refractoriness and source-sink relationship in reentry generation during simulated acute ischemia. *Ann Biomed Eng* 2009 Aug;**37**(8):1560-71.

96. Delgado C, Steinhaus B, Delmar M, Chialvo DR, Jalife J. Directional differences in excitability and margin of safety for propagation in sheep ventricular epicardial muscle. *Circ Res* 1990 Jul;**67**(1):97-110.

97. Wang Y, Rudy Y. Action potential propagation in inhomogeneous cardiac tissue: safety factor considerations and ionic mechanism. *Am J Physiol Heart Circ Physiol* 2000 Apr;**278**(4):H1019-H1029.

98. Jie X, Gurev V, Trayanova N. Mechanisms of mechanically induced spontaneous arrhythmias in acute regional ischemia. *Circ Res* 2010 Jan 8;**106**(1):185-92.

99. Kelly D, Mackenzie L, Hunter P, Smaill B, Saint DA. Gene expression of stretch-activated channels and mechanoelectric feedback in the heart. *Clin Exp Pharmacol Physiol* 2006 Jul;**33**(7):642-8.

100. Craelius W. Stretch-activation of rat cardiac myocytes. *Exp Physiol* 1993 May;**78**(3):411-23.

101. Pollard AE, Cascio WE, Fast VG, Knisley SB. Modulation of triggered activity by uncoupling in the ischemic border. A model study with phase 1b-like conditions. *Cardiovasc Res* 2002 Dec;**56**(3):381-92.

102. Clayton RH, Nash MP, Bradley CP, Panfilov AV, Paterson DJ, Taggart P. Experiment-model interaction for analysis of epicardial activation during human ventricular fibrillation with global myocardial ischaemia. *Prog Biophys Mol Biol* 2011 Oct;**107**(1):101-11.

103. Rodriguez B, Tice BM, Eason JC, Aguel F, Ferrero JM, Trayanova N. Effect of acute global ischemia on the upper limit of vulnerability: a simulation study. *American Journal of Physiology-Heart and Circulatory Physiology* 2004 Jun;**286**(6):H2078-H2088.

104. Rodriguez B, Tice BM, Eason JC, Aguel F, Trayanova N. Cardiac vulnerability to electric shocks during phase 1A of acute global ischemia. *Heart Rhythm* 2004 Dec;**1**(6):695-703.

105. El-Sherif N, Scherlag BJ, Lazzara R, Hope RR. Re-entrant ventricular arrhythmias in the late myocardial infarction period. 1. Conduction characteristics in the infarction zone. *Circulation* 1977 May;**55**(5):686-702.

106. Lue WM, Boyden PA. Abnormal electrical properties of myocytes from chronically infarcted canine heart. Alterations in Vmax and the transient outward current. *Circulation* 1992 Mar;**85**(3):1175-88.

107. Litwin SE, Bridge JH. Enhanced Na(+)-Ca2+ exchange in the infarcted heart. Implications for excitation-contraction coupling. *Circ Res* 1997 Dec;**81**(6):1083-93.

108. Gough WB, Mehra R, Restivo M, Zeiler RH, el Sherif N. Reentrant ventricular arrhythmias in the late myocardial infarction period in the dog. 13. Correlation of activation and refractory maps. *Circ Res* 1985 Sep;**57**(3):432-42.

109. Cabo C, Boyden PA. Electrical remodeling of the epicardial border zone in the canine infarcted heart: a computational analysis. *Am J Physiol Heart Circ Physiol* 2003 Jan;**284**(1):H372-H384.

110. Aggarwal R, Boyden PA. Diminished Ca2+ and Ba2+ currents in myocytes surviving in the epicardial border zone of the 5-day infarcted canine heart. *Circ Res* 1995 Dec;**77**(6):1180-91.

111. Jiang M, Cabo C, Yao J, Boyden PA, Tseng G. Delayed rectifier K currents have reduced amplitudes and altered kinetics in myocytes from infarcted canine ventricle. *Cardiovasc Res* 2000 Oct;**48**(1):34-43.

112. Pinto JM, Boyden PA. Electrical remodeling in ischemia and infarction. *Cardiovasc Res* 1999 May;**42**(2):284-97.

113. Decker KF, Rudy Y. Ionic mechanisms of electrophysiological heterogeneity and conduction block in the infarct border zone. *Am J Physiol Heart Circ Physiol* 2010 Nov;**299**(5):H1588-H1597.

114. Aggarwal R, Pu J, Boyden PA. Ca(2+)-dependent outward currents in myocytes from epicardial border zone of 5-day infarcted canine heart. *Am J Physiol* 1997 Sep;**273**(3 Pt 2):H1386-H1394.

115. McDowell KS, Arevalo HJ, Maleckar MM, Trayanova NA. Susceptibility to arrhythmia in the infarcted heart depends on myofibroblast density. *Biophys J* 2011 Sep 21;**101**(6):1307-15.

116. Peters NS, Wit AL. Myocardial architecture and ventricular arrhythmogenesis. *Circulation* 1998 May 5;**97**(17):1746-54.

117. Dillon SM, Allessie MA, Ursell PC, Wit AL. Influences of anisotropic tissue structure on reentrant circuits in the epicardial border zone of subacute canine infarcts. *Circ Res* 1988 Jul;**63**(1):182-206.

118. Smith JH, Green CR, Peters NS, Rothery S, Severs NJ. Altered patterns of gap junction distribution in ischemic heart disease. An immunohistochemical study of human myocardium using laser scanning confocal microscopy. *Am J Pathol* 1991 Oct;**139**(4):801-21.

119. Kleber AG, Rudy Y. Basic mechanisms of cardiac impulse propagation and associated arrhythmias. *Physiol Rev* 2004 Apr;**84**(2):431-88.

120. Rudy Y. Lessons learned about slow discontinuous conduction from models of impulse propagation. *J Electrocardiol* 2005 Oct;**38**(4 Suppl):52-4.

121. Wilders R, Wagner MB, Golod DA, Kumar R, Wang YG, Goolsby WN, et al. Effects of anisotropy on the development of cardiac arrhythmias associated with focal activity. *Pflugers Arch* 2000 Dec;**441**(2-3):301-12.

122. Monserrat M, Saiz J, Ferrero JM, Jr., Ferrero JM, Thakor NV. Ectopic activity in ventricular cells induced by early afterdepolarizations developed in Purkinje cells. *Ann Biomed Eng* 2000 Nov;**28**(11):1343-51.

123. Rohr S. Myofibroblasts in diseased hearts: new players in cardiac arrhythmias? *Heart Rhythm* 2009 Jun;**6**(6):848-56.

124. Porter KE, Turner NA. Cardiac fibroblasts: at the heart of myocardial remodeling. *Pharmacol Ther* 2009 Aug;**123**(2):255-78.

125. Gaudesius G, Miragoli M, Thomas SP, Rohr S. Coupling of cardiac electrical activity over extended distances by fibroblasts of cardiac origin. *Circ Res* 2003 Sep 5;**93**(5):421-8.

126. Miragoli M, Gaudesius G, Rohr S. Electrotonic modulation of cardiac impulse conduction by myofibroblasts. *Circ Res* 2006 Mar 31;**98**(6):801-10.

127. de Bakker JM, van Capelle FJ, Janse MJ, Tasseron S, Vermeulen JT, de JN, et al. Fractionated electrograms in dilated cardiomyopathy: origin and relation to abnormal conduction. *J Am Coll Cardiol* 1996 Apr;**27**(5):1071-8.

128. MacCannell KA, Bazzazi H, Chilton L, Shibukawa Y, Clark RB, Giles WR. A mathematical model of electrotonic interactions between ventricular myocytes and fibroblasts. *Biophys J* 2007 Jun 1;**92**(11):4121-32.

129. Sachse FB, Moreno AP, Abildskov JA. Electrophysiological modeling of fibroblasts and their interaction with myocytes. *Ann Biomed Eng* 2008 Jan;**36**(1):41-56.

130. Maleckar MM, Greenstein JL, Giles WR, Trayanova NA. Electrotonic coupling between human atrial myocytes and fibroblasts alters myocyte excitability and repolarization. *Biophys J* 2009 Oct 21;**97**(8):2179-90.

131. Xie Y, Garfinkel A, Camelliti P, Kohl P, Weiss JN, Qu Z. Effects of fibroblast-myocyte coupling on cardiac conduction and vulnerability to reentry: A computational study. *Heart Rhythm* 2009 Nov;**6**(11):1641-9.

132. Jacquemet V, Henriquez CS. Loading effect of fibroblast-myocyte coupling on resting potential, impulse propagation, and repolarization: insights from a microstructure model. *Am J Physiol Heart Circ Physiol* 2008 May;**294**(5):H2040-H2052.

133. Jacquemet V, Henriquez CS. Genesis of complex fractionated atrial electrograms in zones of slow conduction: a computer model of microfibrosis. *Heart Rhythm* 2009 Jun;**6**(6):803-10.

134. Petrov VS, Osipov GV, Kurths J. Fibroblasts alter spiral wave stability. *Chaos* 2010 Dec;**20**(4):045103.

135. Engelman ZJ, Trew ML, Smaill BH. Structural heterogeneity alone is a sufficient substrate for dynamic instability and altered restitution. *Circ Arrhythm Electrophysiol* 2010 Apr;**3**(2):195-203.

136. Turner I, Huang H, Saumarez RC. Numerical simulation of paced electrogram fractionation: relating clinical observations to changes in fibrosis and action potential duration. *J Cardiovasc Electrophysiol* 2005 Feb;**16**(2):151-61.

137. Vadakkumpadan F, Arevalo H, Prassl AJ, Chen J, Kickinger F, Kohl P, et al. Image-based models of cardiac structure in health and disease. *Wiley Interdiscip Rev Syst Biol Med* 2010 Jul;**2**(4):489-506.

138. Rantner LJ, Arevalo HJ, Constantino JL, Efimov IR, Plank G, Trayanova NA. Three-dimensional mechanisms of increased vulnerability to electric shocks in myocardial infarction: altered virtual electrode polarizations and conduction delay in the peri-infarct zone. *J Physiol* 2012 Sep 15;**590**(Pt 18):4537-51.

139. Vigmond E, Vadakkumpadan F, Gurev V, Arevalo H, Deo M, Plank G, et al. Towards predictive modelling of the electrophysiology of the heart. *Exp Physiol* 2009 May;**94**(5):563-77.

140. Pop M, Sermesant M, Mansi T, Crystal E, Ghate S, Peyrat JM, et al. Correspondence between simple 3-D MRI-based computer models and in-vivo EP measurements in swine with chronic infarctions. *IEEE Trans Biomed Eng* 2011 Dec;**58**(12):3483-6.

141. Pop M, Sermesant M, Liu G, Relan J, Mansi T, Soong A, et al. Construction of 3D MR image-based computer models of pathologic hearts, augmented with histology and optical fluorescence imaging to characterize action potential propagation. *Med Image Anal* 2012 Feb;**16**(2):505-23.

142. Ng J, Jacobson JT, Ng JK, Gordon D, Lee DC, Carr JC, et al. Virtual electrophysiological study in a 3-dimensional cardiac magnetic resonance imaging model of porcine myocardial infarction. *J Am Coll Cardiol* 2012 Jul 31;**60**(5):423-30.

143. Ashikaga H, Arevalo H, Vadakkumpadan F, Blake RC, III, Bayer JD, Nazarian S, et al. Feasibility of Image-Based Simulation to Estimate Ablation Target in Human Ventricular Arrhythmia. *Heart Rhythm* 2013 doi: 10.1016/j.hrthm.2013.04.015.

Figure legends

Figure 1 Simulation of phase 1A ischaemia at the cellular level. (A) Hypoxic action potentials for different activation degrees of ATP-sensitive K^+ channels. Numbers indicate percentage of open channels. Reproduced from Reference 44 with permission. (B) Time-course of extracellular K^+ concentration during acute ischaemia. Each trace corresponds to a different ionic event: progressive activation of ATP-sensitive K^+ channels ($I_{K(ATP)}$, trace I), inhibition of the Na^+/K^+ pump (I_{NaK}, trace II), activation of an ischaemic slow-activated inward Na^+ current (I_{NaS}, trace III), algebraic sum of the three traces (trace IV), combinations of two mechanisms (traces V to VII) and combination of the three mechanisms (trace VIII). (C) Action potentials from isolated ventricular myocytes at different minutes post occlusion. Panels (B) and (C) modified from Reference 56 with permission.

Figure 2 Simulation of regional phase 1A ischaemia in a two-dimensional tissue. (A) Longitudinal conduction velocity in the normal zone (NZ), border zone (BZ) and central zone (CZ) along the vertical strand depicted in panel E. (B) Effective refractory period (ERP) and action potential duration (APD). (C) Peak Na^+ and L-type Ca^{2+} currents (I_{Na}, $I_{Ca(L)}$). (D) Time-courses of transmembrane potential (V_m), I_{Na} and $I_{Ca(L)}$ in the centre cell. (E) Schematic of the tissue. Reproduced from "Electrical activity and reentry during acute regional myocardial ischaemia: insights from simulations", Ferrero JM, Trenor B, Rodriguez B & Saiz J, *International Journal of Bifurcation and Chaos*, Vol.13(12), © 2003 World Scientific Publishing Company (Reference 72) with permission.

Figure 3 Simulation of phase 1A ischaemia at the organ level. Panels show voltage snapshots (colour-coded membrane voltage) corresponding to the anterior epicardial wall at twelve different instants after the delivery of a premature stimulus. The approximate location of the normal zone (NZ), border zone (BZ) and central ischaemic zone (CIZ) is shown in the first panel. The black line in the third panel shows an arc of block.

Figure 4 Time-course of the vulnerable window duration (VW, panel A) and dispersion of effective refractory period (ΔERP, panel B) during the first 10 minutes of ischaemia. Reproduced from Reference 95 with permission.

Figure 5 Comparison between image-based simulation of chronic myocardial infarction and standard (non-simulation) approach. (A) Activation map of a simulation of ventricular tachycardia (VT). Arrows indicate wave propagation of reentrant circuits, and lines indicate arcs of block. (B) 12-lead ECG of inducible VTs from the standard approach. (C) Three-dimensional CARTO map with colour-coded voltages (purple: normal myocardium; blue, green and yellow: infarct border zones; red: scar) from the standard approach. Circles represent ablation sites. (D) Pre-ablation magnetic resonance imaging showing infarct geometry (orange: scar; yellow: heterogeneous zone; grey: non-infarcted myocardium). The lines of conduction block from the image-based simulation and the ablation sites from the standard approach are co-registered on the heart geometry. (E) Potential target region for ablation (green area) estimated from the image-based simulation. The shortest possible line of ablation that spans the target region is indicated in cyan. The ablation sites that fell within the estimated ablation target (green area) are indicated by yellow circles. Modified from Reference 143 with permission.

Representative figure: Figure 3

Figure 1
Click here to download high resolution image

Figure 1

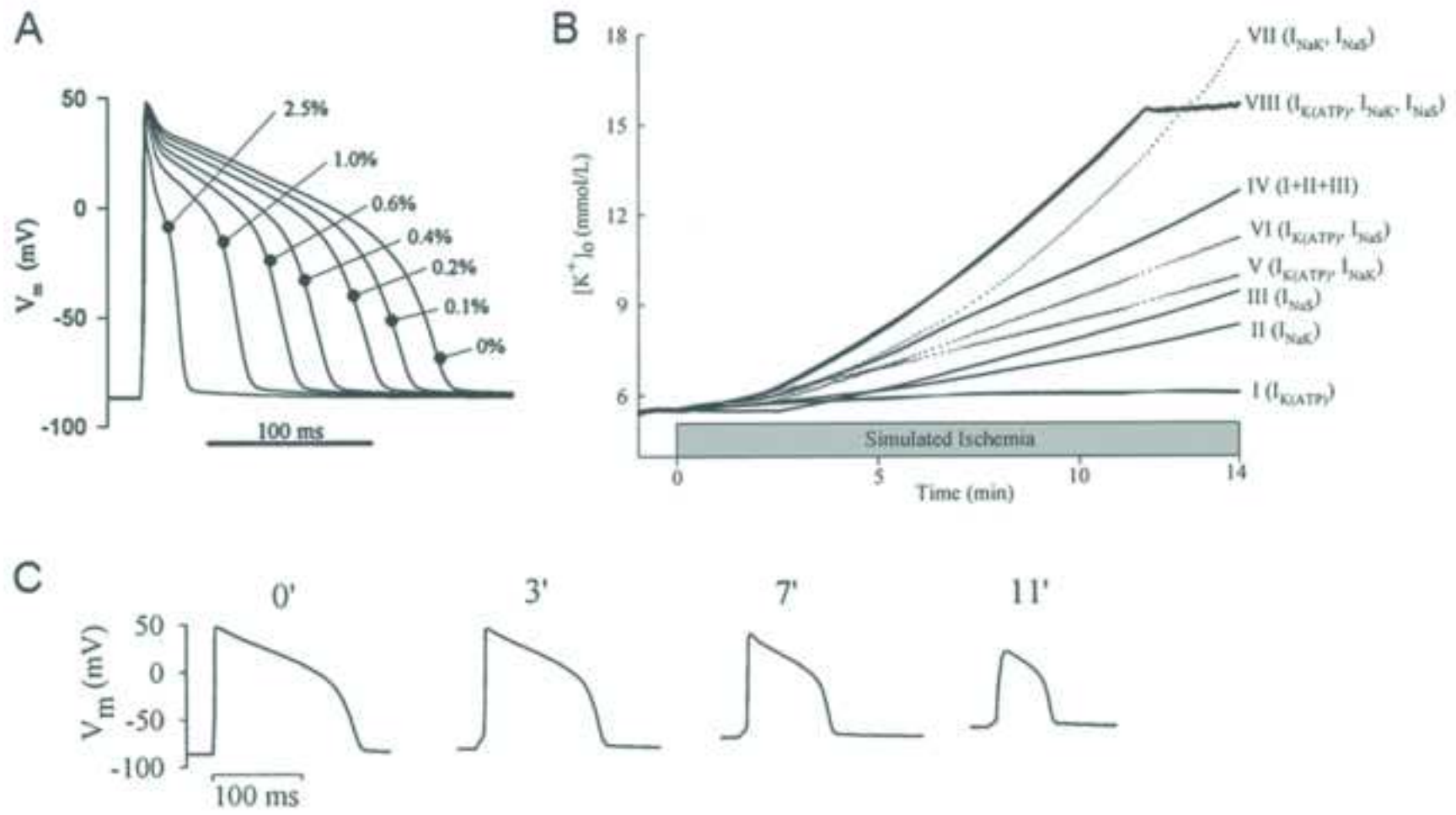

Figure 2
Click here to download high resolution image

Figure 2

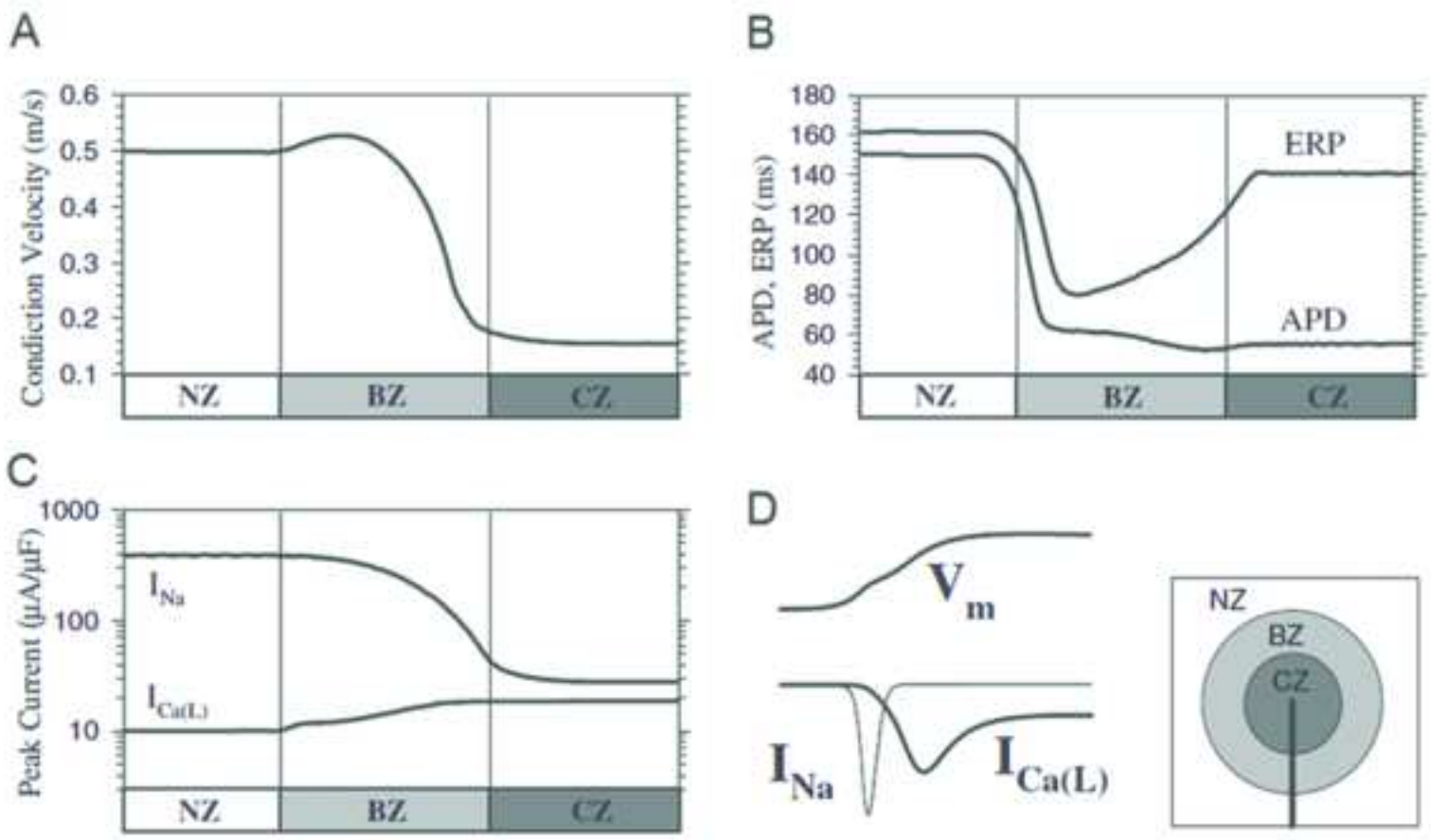

Figure 3
Click here to download high resolution image

Figure 3

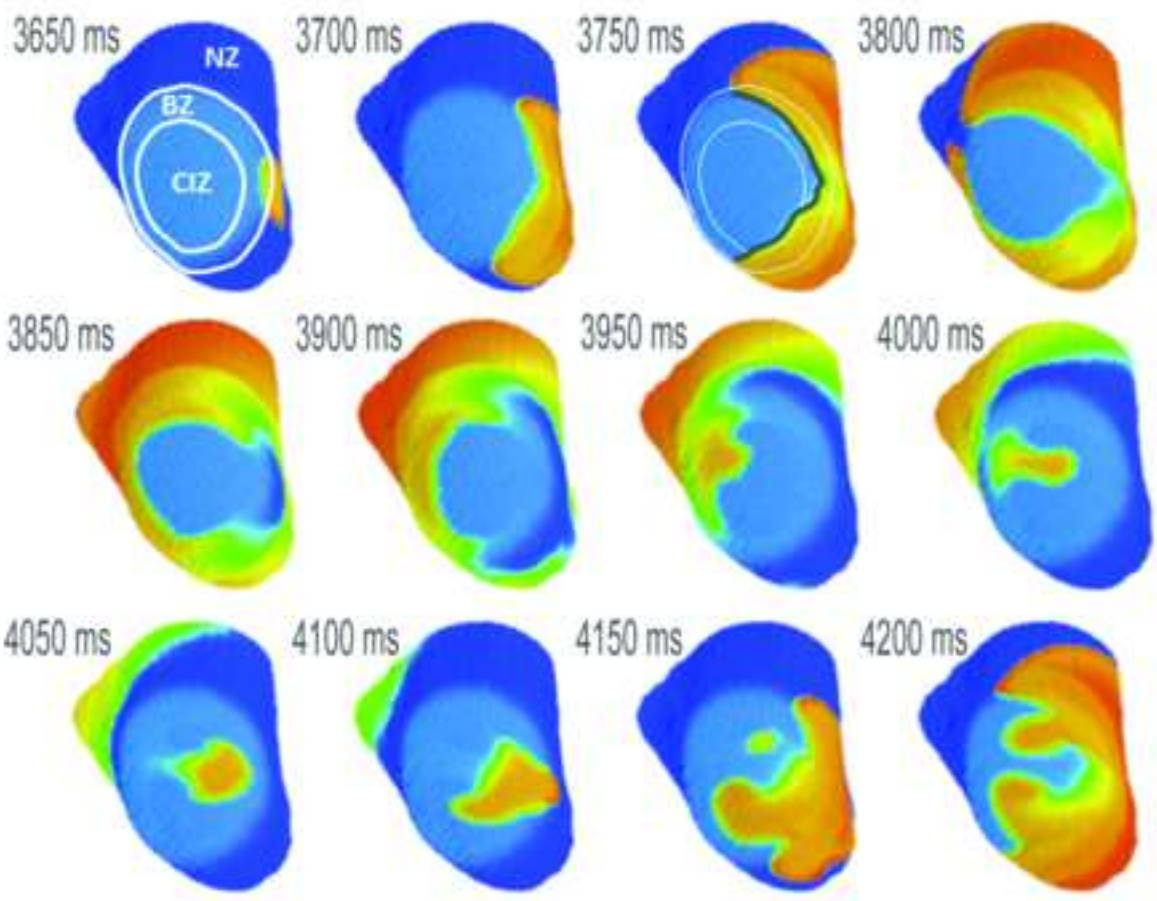

Figure 4
Click here to download high resolution image

Figure 4

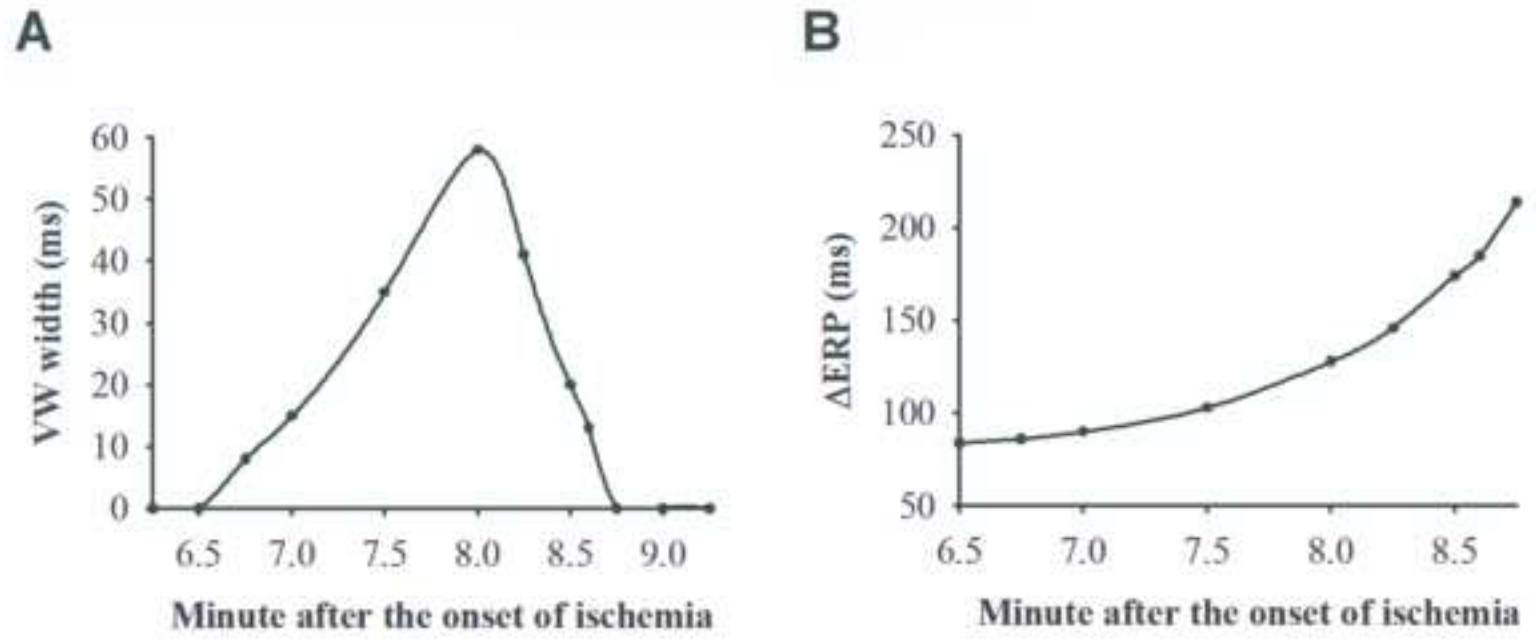

Figure 5
Click here to download high resolution image

Figure 5

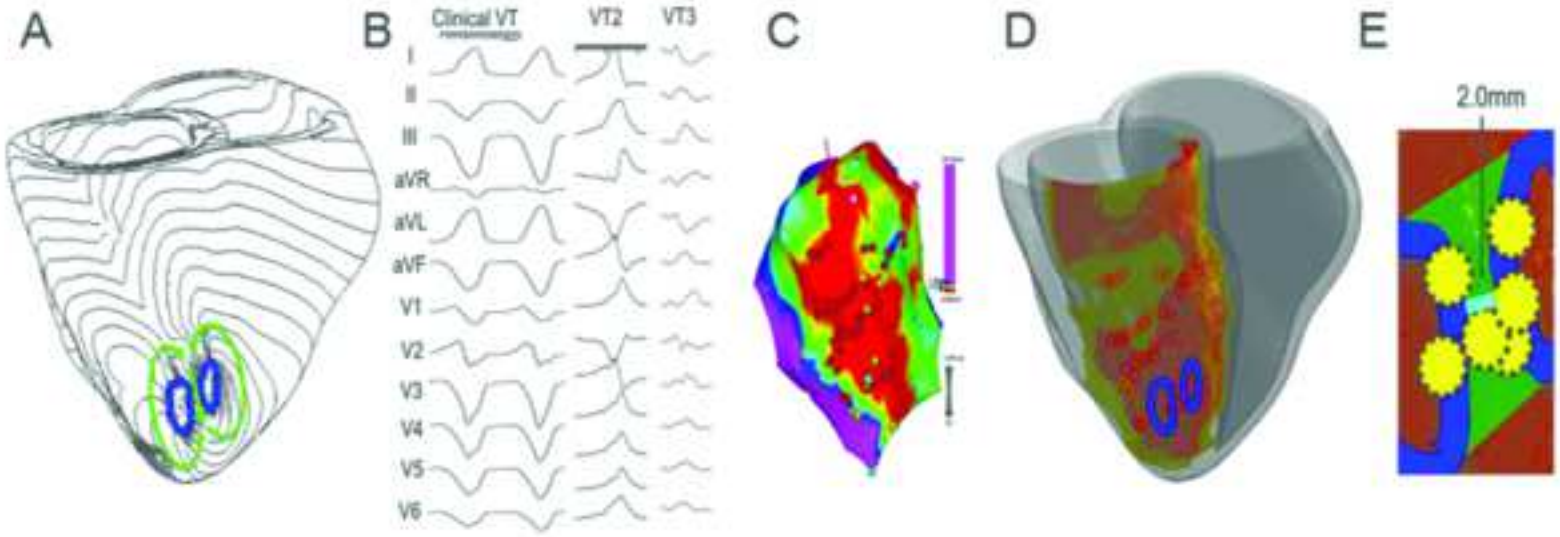

Permissions for reproduction of figures

Click here to download Supplementary file: Persmissions.rar